IBRO Neuroscience Reports 16 (2024) 476–484

Contents lists available at ScienceDirect

IBRO Neuroscience Reports

journal homepage: www.sciencedirect.com/journal/IBRO-Neuroscience-Reports

Research paper

Rat ventral caudal nerve as a model for long distance regeneration

Ivo Vanický [a,*], Juraj Blaško [a], Zoltán Tomori [b], Zuzana Michalová [a], Eva Székiová [a]

[a] Institute of Neurobiology Biomedical Research Center Slovak Academy of Sciences, Šoltésovej 4, Košice 04001, Slovakia
[b] Institute of Experimental Physics Slovak Academy of Sciences, Watsonova 47, Košice 04001, Slovakia

ARTICLE INFO

Keywords:
Peripheral nerve
Ventral caudal nerve
Rat
Injury
Regeneration

ABSTRACT

In the rat, tail nerves are the longest peripheral nerves in their body. We suggest that ventral caudal nerve (VCN) may serve as a model for studying nerve injury and long distance regeneration. For this purpose, we have studied the anatomy and morphometry of the VCN in control animals. 10 cm long segment of the VCN was removed, and transversal sections were collected at 10 mm distances. The myelinated axons were counted, and the series of data were used to characterize the craniocaudal tapering of the nerve. In a separate group of animals, retrograde tracing with Fluorogold was used to localize and quantitate the spinal neurons projecting their axons into the VCN. After complete nerve transection, the time course of histopathological changes in the distal segment was studied. The primary goal was to define the time needed for axonal disintegration. In later periods, axonal debris removal and rearrangement of tissue elements was documented. After compression injury (axonotmesis), Wallerian degeneration was followed by spontaneous regeneration of axons. We show that the growing axons will span the 10 cm distance within 4–8 weeks. After different survival periods, the numbers of regenerating axons were counted at 10 mm distances. These data were used to characterize the dynamics of axonal regeneration during 4 months' survival period. In the present study we show that axonal regeneration across 10 cm distance can be studied and quantitatively analyzed in a small laboratory animal.

1. Introduction

In clinical medicine, repair of injured peripheral nerve remains a challenge. While it is generally accepted that peripheral nerves are capable of regeneration, the clinical outcome of nerve repair is often disappointing (Panagopoulos et al., 2017). It is generally considered that only half of the patients with complete nerve transection regain useful function, and full recovery occurs in less than 10% of the cases (Grinsell and Keating, 2014; Irintchev, 2011). Even more challenging is the nerve reconstruction after segmental injuries, when the gap between the stumps must be bridged either by nerve autografts, or graft alternatives (Carvalho et al., 2019; Konofaos and Ver Halen, 2013). With smaller defect sizes, various bridging techniques can result in successful regeneration. However, with longer distances, the success of axonal regrowth dramatically decreases (Riccio et al., 2019; Sahakyants et al., 2013). This problem occurs with both nerve autografts, and graft alternatives. Currently there is no implant approved for the defect sizes extending 3 cm (Pan et al., 2020; Kornfeld et al., 2019). Therefore, repair of long nerve gaps remains an unmet need in clinical practice and a key research challenge. However, in experimental literature, there are very few studies that would systematically study the mechanisms responsible for regeneration failure in the grafts longer than the critical distance. In rodents, most of the peripheral nerve injury/regeneration studies have been performed on sciatic nerve that is the largest nerve in the body (Irintchev, 2011; Kaplan et al., 2015). However, there are some drawbacks associated with the sciatic nerve model. After transection, the denervation of the whole hindlimb elicits autophagy in some animals, which is very difficult to prevent (Weber et al., 1993). In addition to ethical aspects of this complication, a fraction of animals must be eliminated from the study. The length of the nerve does not allow creating long segmental injuries similar to those that are critical in human patients. In addition, the complicated branching of the nerve on its trajectory to the periphery makes the visualization (and quantification) of the regenerating axons technically difficult. Presence of the new axons is therefore usually documented at very short distances below the site of injury (Angius et al., 2012).

We suggest that rat VCN can be a useful alternative for studying long segmental injuries, and for comparing the outcomes after various repair techniques. The nerve is straight, and at least 10 cm long segment in the tail is easily accessible for both surgical interventions and histological

* Corresponding author.
E-mail address: vanicky@saske.sk (I. Vanický).

https://doi.org/10.1016/j.ibneur.2024.03.008
Received 27 November 2023; Accepted 15 March 2024
Available online 22 March 2024

analyses. The transection of VCN does not cause visible discomfort to the surviving animals and no autophagy was observed during our experiments.

In the present study, we characterize the morphological details of the VCN in control animals, and identify the neuronal pools within the spinal cord that project their axons into VCN. In experiments with two different types of injury we have documented: i, after transection, the time course of axonal disintegration in the distal stump, and ii, after axonotmesis, the growth of the regenerating axons. After different survival periods, myelinated axons were counted at regular distances, and the data were used to document the regeneration process.

These data form a basis for future studies on various nerve injury/repair strategies. The progress of axonal regeneration after different ways of nerve reconstruction can be evaluated quantitatively, and even subtle differences in the numbers and distances of axonal regeneration can be detected. We believe that this model can help to generate the data needed for better understanding of the mechanisms responsible for axonal regeneration failure after critical distance repairs.

2. Experimental procedures

The experiments were carried out in accordance with European Council Directive (2010/63/EU) and approved by the State Veterinary and Food Administration of the Slovak Republic (1360/18–221–3) under the supervision of the ethical council of the Institute of Neurobiology BMC SAS. Every effort was made to minimise animal suffering and reduce the number of animals used. Adult male albino Wistar rats (bred at a certified vivarium of the Institute of Neurobiology BMC SAS originating from Velaz, Czech Republic) weighing 290–330 g were maintained on a 12 h light/dark cycle and given food and water ad libitum.

2.1. Experimental groups

1. control group, nerve anatomy and morphometry. In control group (n=5), the animals were sacrificed by inhalation of 5% isoflurane. Along the whole tail, lateral skin incision was made at one side. The wound was wide opened using several skin retractors. Under operating microscope, the VCN was isolated at the tail base and then caudally dissected free from the surrounding tissues. As the axons are sensitive to compression artifacts, we sought not to squeeze the nerve by instruments. After at least 11 cm long segment of nerve was isolated, its distal end was ligated and transected. By holding the ligature, the nerve was gently lifted up, small segmental branches were cut by ophtalmic scissors and the whole nerve trunk was removed. The stretched nerve was immersion fixed in a large Petri dish filled with 2.5% glutaraldehyde in 0.1 M phosphate buffer (pH=7.4). After nerve harvesting, dissection of proximal segments of both caudal nerves was made, and their course in the lower back region was traced cranially up to the spinal cord.

2. retrograde tracing group, visualization and quantification of motoneurons. Animals (n=5) under inhalation anesthesia were placed in lateral position. Lateral skin incision (approx. 2 cm) was made at the tail base. Under operating microscope, the left VCN was exposed and transected with ophtalmic scissors 1 cm below the tail base. Its proximal stump was inserted approx. 1 mm deep into a 5 mm long tube (1 mm I. D., mPES) that was attached to epineurium with a tissue adhesive (Histoacryl Flexible, B. Braun). The attached tube was filled with 4% Fluorogold (Fluorochrome) and its distal end was closed with a silon insert, secured with a droplet of tissue adhesive. Tendons were sutured with silk (Silk braided, EP 0.5 Chirana, T.Injecta), and the skin was closed with continuous horizontal mattress suture (Tervalon braided, EP 1.5, Chirana, T.Injecta). After 7 days' survival, the animals were reanesthetized, and transcardially perfused (saline and 4% paraformaldehyde in 0.1 M PB). Spinal cords were removed from the bone, dura mater was opened and the caudalmost part of the spinal cord (L6 – end of conus terminalis) was isolated. The whole specimen was made translucent after clearing procedure (Zygelyte et al., 2016). Briefly, the tissue was first dehydrated in ascending grades (50–100%) of tetrahydrofuran (Sigma-Aldrich) for 30 minutes in each concentration, then incubated in 100% dichlormethane (Sigma-Aldrich) for 20 minutes and in 100% dibenzyl ether (Sigma-Aldrich) for 30 minutes. The cleared specimen was whole-mounted with dibenzyl ether on a histological slide and observed under fluorescent microscope (Olympus BX-50) using wide band ultraviolet excitation filter.

3. nerve transection group, time course of axonal disintegration. In anesthetized animals (n=8),VCN was isolated and transected 1 cm below the tail base with ophtalmic scissors. The proximal stump was tightly ligated with a non-absorbable ligature (braided polyester, Tervalon EP 1.0, Chirmax) in order to prevent spontaneous regeneration. The wound was sutured as described above. The animals were allowed to survive for 1(n=2),2(n=2), 4(n=2) and 8(n=2) weeks. After survival period, the animals were sacrificed as described above and the distal stump of the transected nerve was removed and immersion fixed for histological analyses.

4. axonotmesis group, quantitative analyses of axonal regeneration. The animals (n=14) were anesthetized, VCN was isolated and crushed at the tail base with a microsurgery needle holder with smooth jaws (width 1 mm). After crush, the injury site was observed under stereomicroscope. The two stumps of the crushed nerve are separated, but the flattened epineurium and other connective tissues form a bridge between the stumps. Within 10 minutes, the crushed segment slowly becomes filled with transparent exsudate. The wound was then sutured and the animals were allowed to survive for 2(n=3),4(n=3), 8(n=4) and 16(n=4) weeks. After survival period, the animals were sacrificed as described above, the nerve was removed and immersion fixed.

2.2. Nerve embedding, sampling and histological processing

After overnight fixation, the nerve was transferred into 0.1 M phosphate buffer. Under stereomicroscope, loose membraneous sheets were carefully removed. The whole nerve was then embedded into albumin matrix (Vanicky et al., 2022). Briefly, the stretched nerve was encircled with silicone blocks and the mold was filled with a mixture of albumin/concentrated formaldehyde. After overnight hardening in a moisture chamber, the hardened block was removed, placed into a metallic Tissue matrix (TM-1000 10×10 mm chamber w/1 mm slices, ASI Instruments, USA), and cut with a microtome blade into 1 mm thick slabs. In this way, a series of 1 mm thick transversal slabs can be prepared from the whole specimen. The selected slabs were trimmed, osmificated, dehydrated and embedded into Durcupan. 1–3 μm thick transversal sections were cut on a standard sliding microtome (Leica SM2010R) equipped with special blade for hard tissues (Feather HR35), and teased onto gelatinized slide from 96% ethanol. The sections were either coverslipped with Polymount unstained for routine screening, or stained with a modified Richardson's stain (Dzurjaskova et al., 2021).

2.3. Axonal counting

From each section, high resolution micrographs were prepared. The images were analysed with custom-made image analysing software developed by Z.T. The software enables systematic random sampling of the cross-sectional area, automatic detection of the objects of interest (myelinated axons), and manual corrections. A typical analysis of a section containing approximately 2000 axons can be completed within 10 minutes. The software is freely available at: https://home.saske.sk/~tomori/software/NeuroCounter.html

3. Results

3.1. Ventral caudal nerve gross anatomy

Both dorsal and ventral caudal nerves are formed from spinal nerves

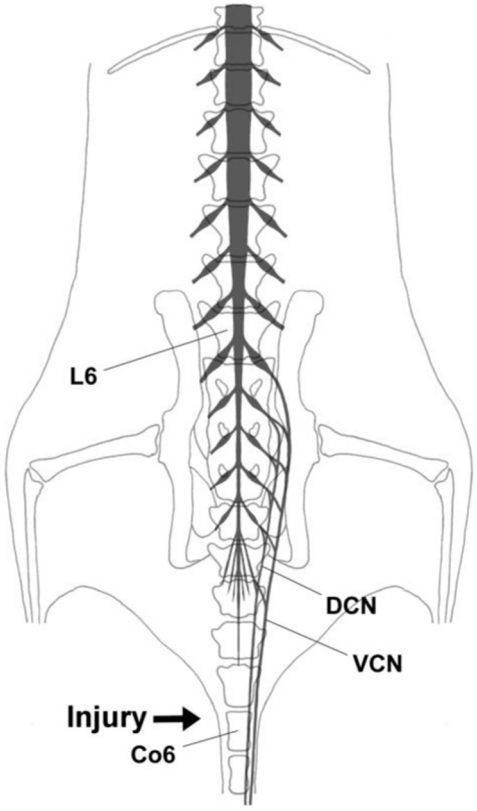

Fig. 1. Schematic drawing of the anatomy of spinal nerves forming the caudal nerves. The spinal nerves split into dorsal and ventral branches. The branches from individual segments merge and give rise to dorsal and ventral caudal nerves.

L6, S1-S4 and Co1. These spinal nerves split into dorsal and ventral branches. Both branches run caudally, segmental branches merge and form the dorsal and ventral caudal nerves (Fig. 1). The caudal nerves run in the lower back before entering the tail. In the lower back, the DCN lies on the top of the transverse processes of the coccygeal vertebrae. In the tail, it runs under the long tendons in the upper quadrant of the tail. The VCN passes under the posterior pelvic wall and enters the tail under the transverse processes of the coccygeal vertebrae. In the tail, VCN runs under the long tendons in the lower quadrant. Both nerves are sending off small segmental branches that, after being formed, run for several millimeters together with the main trunk of the nerve. The lower back segment of the VCN is approximately 5 cm long, and in the tail approximately 16 cm long segment can be dissected (because of the small diameter, we usually ended dissection approx. 3 cm before the tip of the tail) (Fig. 2). The length of the whole VCN thus reaches more than 20 cm in adult rats.

Surgical access to the VCN: For practical purposes, we have defined the base of the tail as the point where the hairy skin of the back turns into squamous skin of the tail. Skeletopically, this point corresponds to Co6 vertebrae. On the tail, the caudal nerves can be accessed through longitudinal lateral skin incisions. After skin opening, arrays of longitudinal tendons are visible, organized into dorsal and ventral group, dividing the tail into quadrants. The VCN trunk can be best accessed after opening the space between the first and second tendon in the ventral quadrant. The nerve trunk itself is enclosed in a loose membraneous sheath, that can be opened by sharp tweezers (Canta et al., 2010). For morphometric analyses, we have routinely isolated at least 11 cm long segments of the nerve.

3.2. VCN morphometry and axonal counts

On transversal sections, the VCN trunk has a round shape. At the tail base, the nerve diameter (without epineurium) is approx. 0.4 mm, and it contains 1926±75 myelinated axons. Caudally, the nerve gets gradually tapered as it sends off small segmental branches. At the distance 100 mm from the tail base, the diameter of the nerve trunk is approx. 0.2 mm and contains 439±38 myelinated axons. Cross-sectional areas and axonal counts at 11 levels are presented in Fig. 3.

3.3. Retrograde tracing of the motoneurons in the spinal cord

Fluorogold positive motoneurons were detected on ipsilateral side of the spinal cord. Positive cell bodies were clearly distinguishable after tissue clearing, distributed within the ventral grey column of the spinal cord (Fig. 4). The labelled cells were scattered within the 18–20 mm long caudalmost segment of the spinal cord, which corresponds to levels from S1 to the end of conus medullaris. Quantification has revealed an average number of 178±16 positive cells.

3.4. Nerve transection – the time course of axonal disintegration in the distal stump

The patterns of tissue changes after nerve transection are shown on Fig. 5. After 1 week there is marked reduction of axonal profiles and the tissue contains mix of degenerated and intact axonal structures. After 2 weeks there is practically complete disintegration of normal myelinated axons within the tissue. The tissue contains high numbers of dark myelin clumps and only a few myelin rings at different stages of disintegration. The empty spaces become filled with pale newly formed cells. After 4 weeks the myelin clumps are still present, but are reduced in both number and size. At this stage the tissue contains no elements that might be mistakenly considered as axonal profiles. After 8 weeks there are only a few dense myelin clumps remaining in the tissue. The mosaic pattern of the nerve tissue remains preserved, and becomes very distinctive at this stage. The basal membrane-formed units that enveloped individual myelinated axons are densely packed with pale cells, and the fasciculi contain dark intercalated cells.

Axonotmesis – growth of regenerating axons. Histological observations confirmed completeness of axonal injury in all animals. After 2 weeks, no regenerating axons were detected at the systematically analysed distances (10 mm +). However, in the segments adjacent to the site of injury structures resembling newly sprouting axons can be observed up to 7 mm from the site of injury. At the highest magnification, these structures appear as pale droplets. They became enveloped by Schwann cells and in many cases, one Schwann cell engulfed more than one droplet-like structure. After 4 weeks, many growing axons can be found in the segments up to 50 mm below the site of injury. The axons are round, with a thin myelin, and stand sharply out against the diffuse background. At this stage, the numbers of axons are lower than those in

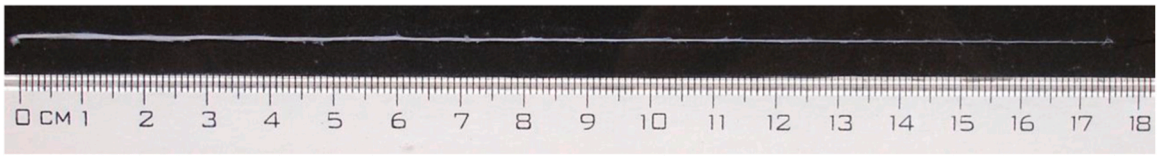

Fig. 2. Dissected ventral caudal nerve - more than 17 cm long segment can be isolated for experimental interventions and analyses.

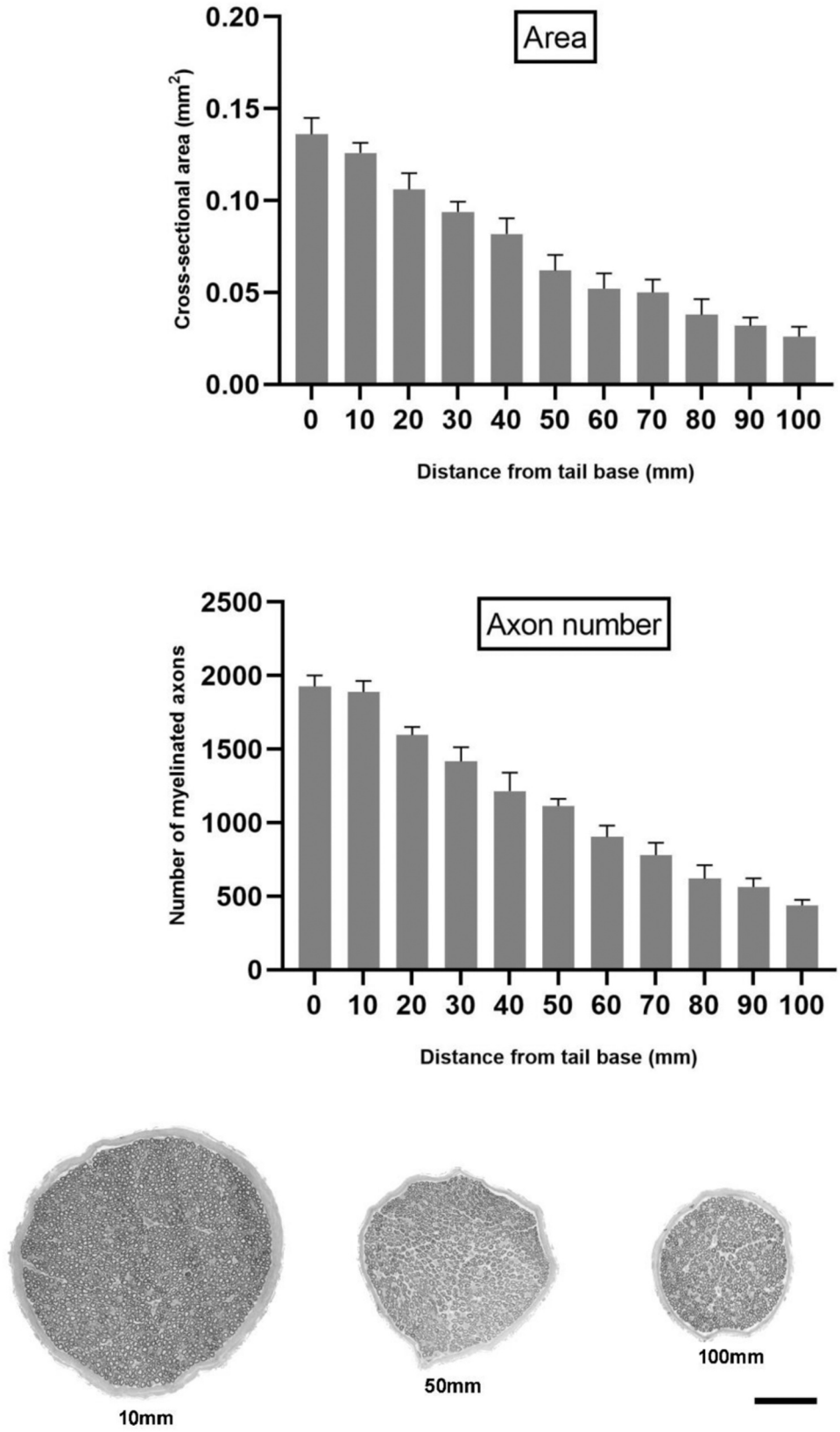

Fig. 3. Morphometric data characterizing the 100 mm long segment of the VCN. Cross sectional areas were measured and numbers of myelinated axons counted on 1 μm thick resin sections. Three representative sections collected at 10, 50 and 100 mm distance are shown. Scale bar=100 μm.

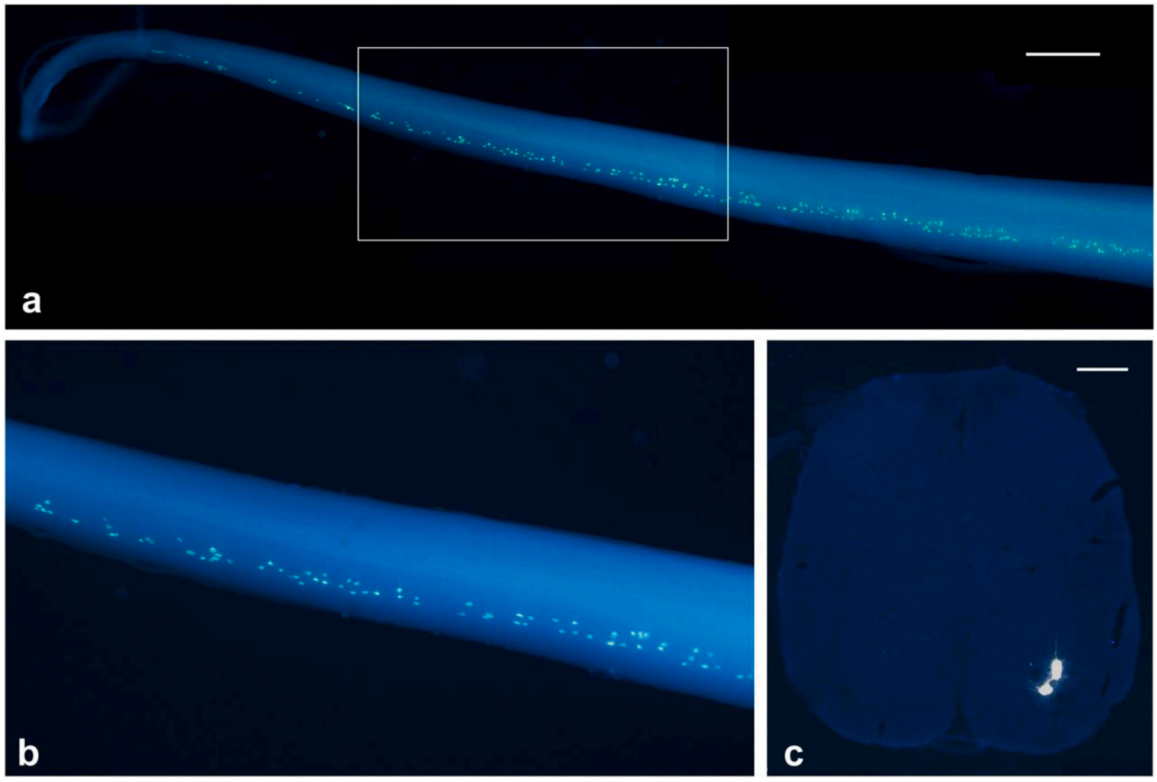

Fig. 4. a), b) – whole-mount preparation of the spinal cord (L6-conus terminalis). a) montage of micrographs to document the whole region containing the labeled motoneurons. Scale bar=1000 μm. b) magnified insert from a. c) appearance of labeled neurons at transversal section. Only motoneurons were labeled.

intact animals at all levels. After 8 weeks, new axons can be seen at all analysed distances. Their myelin sheaths become thicker, and their shape resembles the picture seen in control animals. The numbers of axons are higher than in control animals at all distances. After 16 weeks, the numbers of axons become reduced and seem to return to control values at the levels close to the site of injury. In the more distant regions, the numbers remain elevated, see Fig. 6 and Fig. 7.

4. Discussion

In the rat, tail nerves have been used mainly in electrophysiological experiments (Canta et al., 2010; Leandri et al., 2008; Leandri et al., 2007; Loffredo et al., 2009). In the present study, we show that VCN is accessible for surgical interventions, and long segments of the nerve could be removed for systematic histological processing. Therefore, it can be a used as a model for studying axonal injury and regeneration for long distances. In control animals, we have documented morphometric characteristics of the 10 cm long segment of VCN. The morphology of this nerve is specific, as it forms a long tapering trunk, sending out fine segmental branches. In the analysed segment of the nerve, samples were collected at 10 mm distances. Systematic sampling of such a long and fragile tissue specimen was challenging. It was greatly facilitated by a non-penetrating embedding method developed in our laboratory (Vanicky et al., 2022). The embedded specimen forms a semi-solid block that can be placed into a tissue matrix and cut into a series of 1 mm thick slabs. These slabs with regular thickness were optimal for osmification, resin saturation and proper orientation for transversal sectioning. A series of axonal counts at 10 mm distances was used to characterize the nerve anatomy in control animals.

In a separate group of animals, Fluorogold neuronal tracing was made in order to quantitate the neurons that project their axons into VCN at the level where we are planning to perform injuries (i.e. 1 cm below the tail base). After tissue clearing, the whole sacrocaudal spinal cord could be analysed as a single whole-mount preparation. This procedure eliminated laborious serial sectioning and counting bias. The number of labeled neurons was approx. 180. The transected nerve contains approx. 1900 myelinized axons. This means that the motor component in VCN is significant. We assume that the VCN contains both motoric and sensitive fibers. This assumption is based on our observation of microglial reaction in the spinal cord dorsal horn after VCN injury (unpublished data), but at this time we do not know exactly the ratio of sensitive and motor component. VCN model thus can be used to study regeneration of both motor and sensory axons.

In a nerve transection experiment, we wanted to document in detail the time course of axonal disintegration. It is known, that after axotomy, there is a period during which the axons remain structurally intact, and axonal debris can remain in the denervated tissues for relatively long periods. Therefore, we wanted to define the "safe"period when the distal stump contains no more structures that might be mistakenly counted as regenerating axons. We have found that after 2 weeks, the tissue contains practically no myelinated axons with normal structure, but there were some vacuoles that resembled weakly myelinated axons. After 4 weeks, no myelinated axon-resembling structures were observed. In general, during the first 4 weeks, a process of axonal disintegration and debris clearing takes place. After longer survival periods, the tissue was deprived of axons but still appeared very vital. Its compartmental organization was preserved and became densely repopulated primarily by proliferating Schwann cells. These changes were similar in both proximal and distal regions of the denervated nerve stump, indicating that the degeneration process progresses uniformly, irrespective of the distance from the site of injury.

After axonotmesis, we observed spontaneous regeneration of axons and characterized the dynamics of the regeneration process during 16 weeks' survival. We observed sprouting axon-like structures already after 2 weeks just below the injury site. However, it should be taken into consideration that such fine structures cannot be identified unequivocally. Our interpretation of the droplets as fine tips of regenerating axons was mainly based on the fact that no such structures were observed in

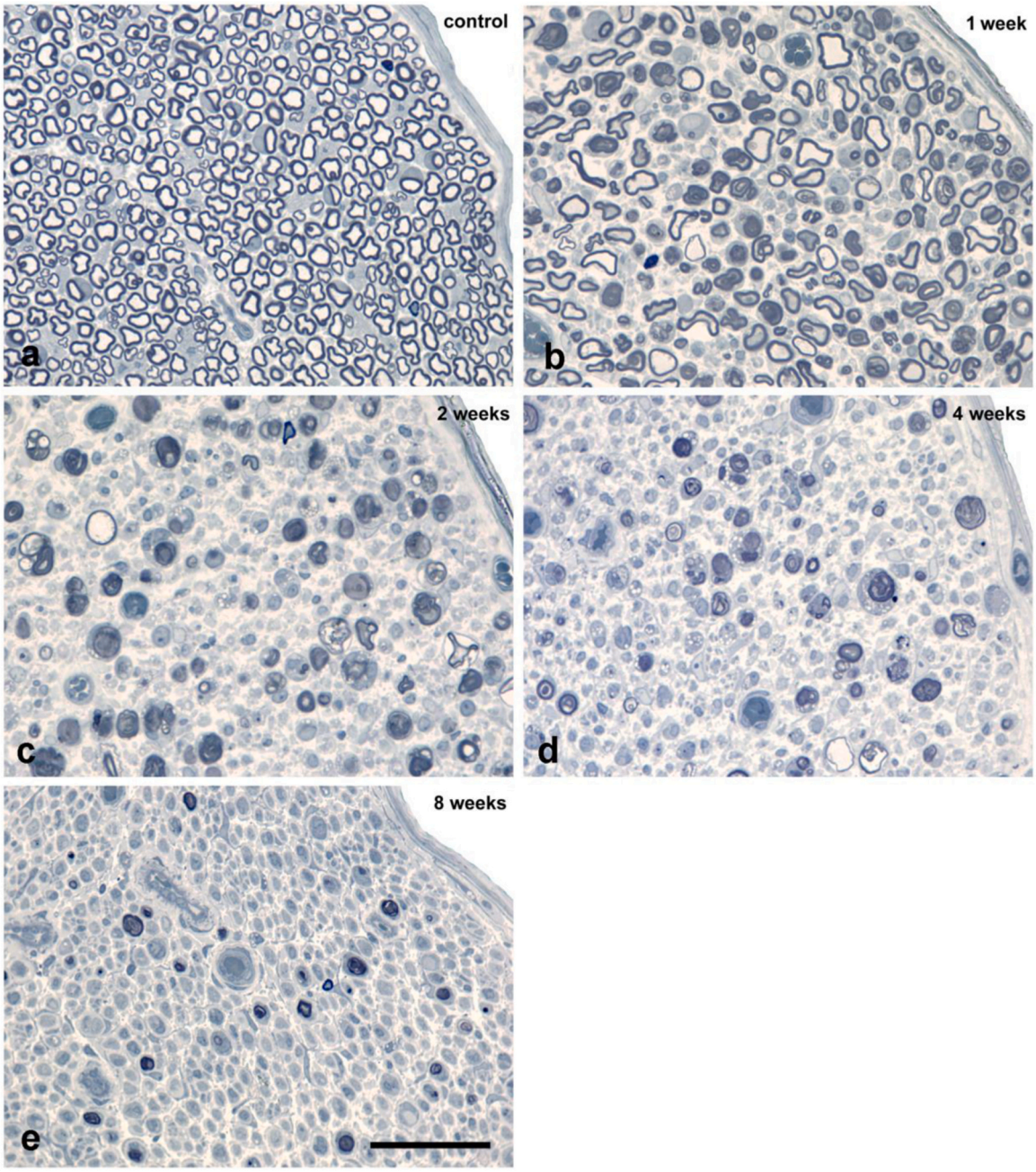

Fig. 5. Wallerian degeneration – development of pathomorphological changes in the distal segment after transection; different survival periods. 1 μm thick Durcupan sections, Richardson's staining, oil immersion. Scale bar=50 μm.

animals after nerve transection.

Within 8 weeks, new axons were observed at all levels, and their numbers were higher than those in control animals. After 16 weeks, the numbers of axons returned to control values at the distances close to the site of injury, indicating elimination of axons that failed to establish contact with their targets. From these observation, we have calculated the rate of the fastest growing axons to be 1.8 mm/day. This corresponds well with the assessed growth rates (1–2 mm/day) published in other studies {Grinsell, 2014 #3}. In comparable experiment with sciatic nerve axonotmesis, Wang et al. observed after 28 days, at 5 mm below the site of injury the number of myelinated axons was approx. 65% compared to intact control {Wang, 2023 #51}. In our experiments after 28 days, at 10 mm below the site of injury the number of axons was approx. 60%. This indicates that the rate of growth is similar to that observed in sciatic nerve experiments.

Functional consequences of VCN transection are modest. In fact we have tried several tests to document functional deficit after VCN transection, but we could not detect any reliable and quantifiable outcomes. It seems that overall movements of the tail are controlled by the muscles located (and innervated) above the tail base. At the present, we cannot quantitate funcional loss and recovery after VCN transection.

The data collected from our series of experiments confirm that VCN can be used for modelling nerve injury and for quantitative evaluation of the regeneration process within a 10 cm long segment of peripheral nerve. We believe that this model can be useful for studying various modes of nerve repair after segmental injuries.

In clinical practice, large segmental injuries represent the most challenging form of nerve injury (Wang et al., 2023). The best possibility for large defect repair remains a nerve autograft (Pan et al., 2020; Kornfeld et al., 2019). In both experimental and clinical studies, it has

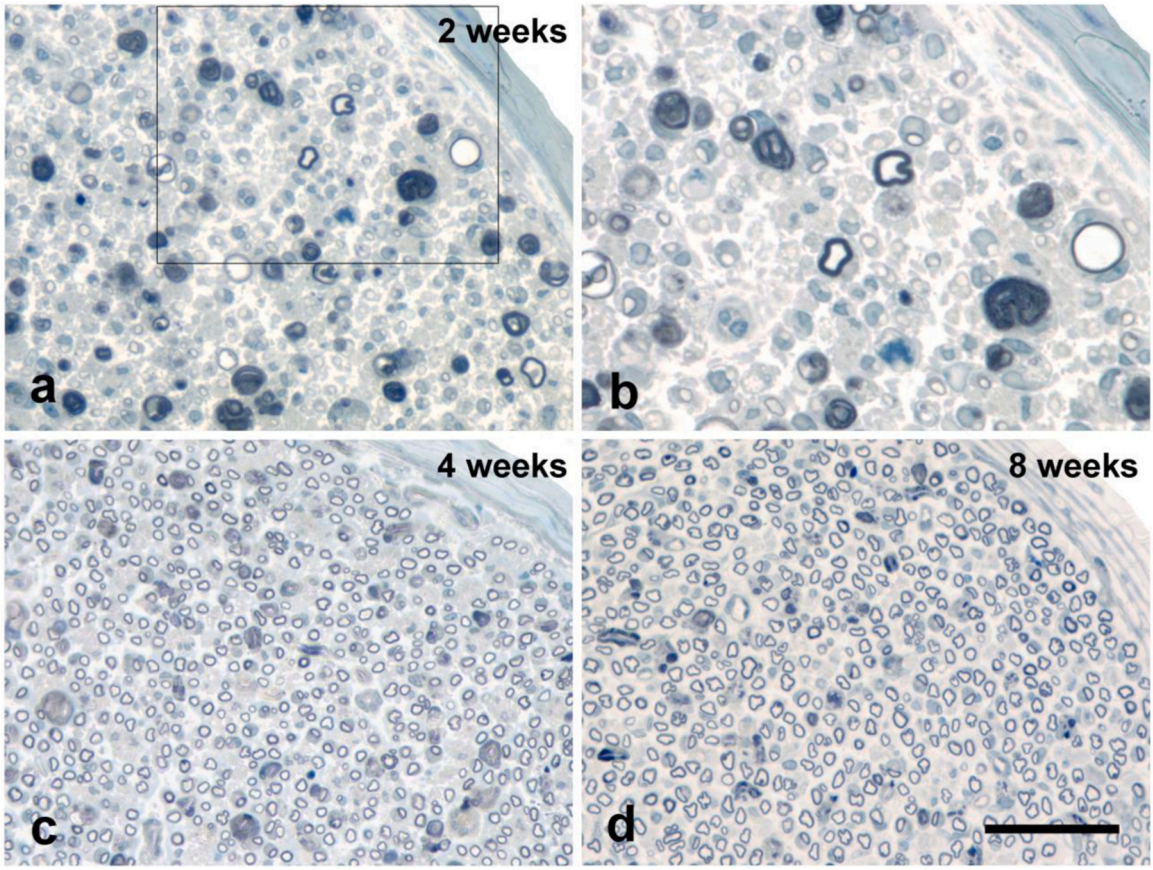

Fig. 6. Growth of new axons within the distal stump of the nerve after axonotmesis. 1 μm thick Durcupan sections, unstained, oil immersion. Scale bar=50 μm. a) and b) 2 weeks survival. Combination of Wallerian degeneration and growth of unmyelinated (or very lightly myelinated) axons. At high magnification 100x objective b), new axons appear as pale droplets. Most of them are encircled by dedifferentiated Schwann cells. One Schwann cell often envelop more than one axon. c) 4 weeks survival. All new axons become slightly myelinated, are round shaped and smaller than normal axons. d) 8 weeks survival, the axons are bigger, myelination is stronger and their shape is more variable, similar to nerves from control animals.

been documented that there is clear relationship between defect length and recovery rate (Scholz et al., 2009; Kallio, 1993). There is no consensus on the maximum gap that can be bridged, and varying degrees of success have been reported after autograft reconstructions up to 200 mm. But there is a general consensus that consistent recovery cannot be expected when autografts are longer than 60 mm (Pan et al., 2020).

Autograft alternatives (processed nerve allografts or nerve guidance channels) can support regeneration similar to autografts for short distances (Koller et al., 1997). However, with large gaps, they can fail to facilitate any nerve regeneration across a bridged nerve defect. At present, all available nerve graft alternatives are approved for repairs of gaps not exceeding 30 mm (Kornfeld et al., 2019).

As axons are capable to regenerate for long distances in optimal conditions, further research should focus on better understanding of the biological mechanisms responsible for regeneration failure in long grafts.

One of the problems in this field is difficulty with modelling long distance regeneration. Obviously, large animal models could be used. In fact, several nerve injury experiments have used large laboratory animals including cats, dogs, sheep, swine, and primates (Kornfeld et al., 2019; Rbia and Shin, 2017). However, experiments with large animals are very demanding, and currently there is no established model that would be used as a standard for large scale experiments.

Vasudevan et al. have introduced an interesting alternative. They developed a rat model for reconstruction of long nerve gap defects by transecting the sciatic nerve and implanting either long isografts or nerve guidance channels in a looped configuration to accommodate the long length (Calancie et al., 2009). They documented that there is robust regeneration across 4 cm long isografts. Later, Saheb-Al-Zamani et al. used this model for studying the critical distances for repair with isografts and acellular nerve allografts (ANAs), up to 6 cm. They have observed reliable regeneration with isografts. In contrast, within ANAs the regenerating axons grew for several millimeters, but the growth stopped after 4 weeks. Interestingly, they have found inverse relationship between the distance of axonal regeneration and ANA graft length, indicating that in long grafts, there must be a significant change in the local regenerative environment that actively halts regeneration. They indicated that senesce changes in cells that newly populate the long ANAs can be a critical factor (Vasudevan et al., 2013).

Poppler et al. used long ANAs, implanted for 4weeks to generate short grafts that are normally permissive for regenerating axons (Poppler et al., 2016). They observed that after implantation, the short "stressed " ANAs were inhibitory for axonal regeneration. Conversely, when the distal segment of long ANAs was after 4 weeks replaced by fresh isografts, the axons were "rescued" and continued to cross the entire 6 cm gap. These results demonstrated that in long ANAs, the environment has been altered so that it is inhibitory for axonal growth. Importantly, the axons retained their inherent ability to grow (Saheb-Al-Zamani et al., 2013). These important insights into neurobiology of nerve regeneration across long gaps have been enabled by "looped graft" implantation model.

In our experiments, we demonstrate that VCN in the rat allows observation and quantitation of axonal regeneration across 10 cm distance. We believe that this model might be useful as it has all the advantages of small animal models, and allows studying axonal

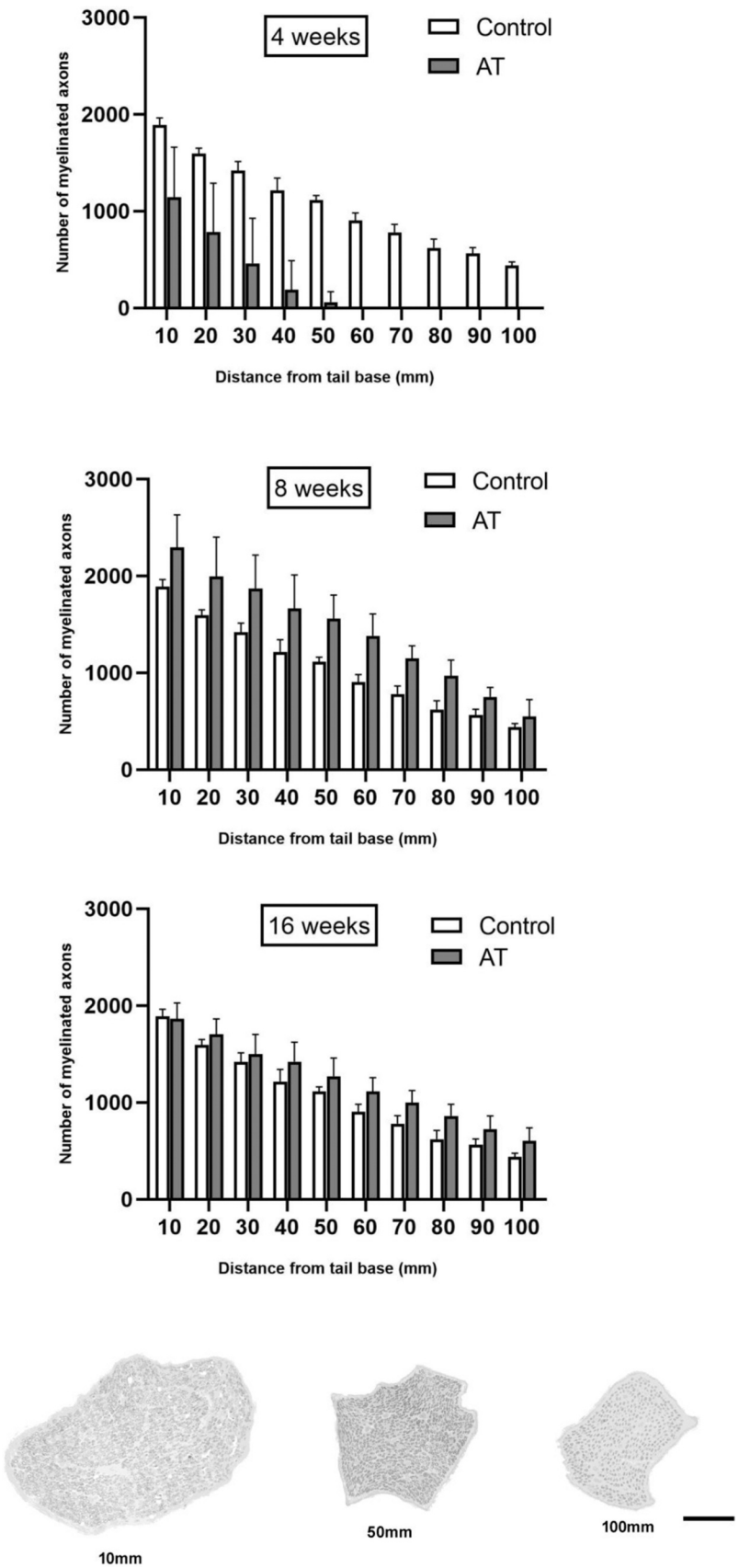

Fig. 7. Regeneration of axons after axonotmesis. Axonal counts within a 10 cm long segment of VCN at different survival periods, compared to counts in intact nerves (Control). Data at point 0 (crush site) were omitted as axons are not arranged in one direction (disordered growth). Appearance of regenerated axons after 16 weeks survival is shown at three representative sections collected at 10, 50 and 100 mm distance. Scale bar=100 μm.

regeneration across distances that surpass the critical distances in human patients. We believe that it can be useful for studying the limits of regeneration within different types of grafts and nerve guidance conducts.

CRediT authorship contribution statement

Ivo Vanický: Conceptualization, Methodology, Writing, **Juraj Blaško**: Methodology, Data curation, **Zoltán Tomori**: Software development, **Zuzana Michalová:** Data processing, Validation, **Eva Székiová**: Data processing, image analyses

Declaration of Competing Interest

None.

Acknowledgements

Funding: Projects VEGA 2/0120/23, 2/0109/21, 2/0101/22, APVV-21-0333, APVV-19-0279.

References

Angius, D., Wang, H., Spinner, R.J., Gutierrez-Cotto, Y., Yaszemski, M.J., Windebank, A. J., 2012. A systematic review of animal models used to study nerve regeneration in tissue-engineered scaffolds. Biomaterials 33, 8034–8039.
Calancie, B., Madsen, P.W., Wood, P., Marcillo, A.E., Levi, A.D., Bunge, R.P., 2009. A guidance channel seeded with autologous Schwann cells for repair of cauda equina injury in a primate model. J. Spinal Cord. Med 32, 379–388.
Canta, A., Meregalli, C., Chiorazzi, A., Carozzi, V.A., Crippa, L., Marmiroli, P., Cavaletti, G., 2010. The ventral caudal nerve: a physiologic-morphometric study in three different rat strains. J. Peripher Nerv. Syst. 15, 140–146.
Carvalho, C.R., Oliveira, J.M., Reis, R.L., 2019. Modern trends for peripheral nerve repair and regeneration: beyond the hollow nerve guidance conduit. Front Bioeng. Biotechnol. 7, 337.
Dzurjaskova, Z., Blasko, J., Tomori, Z., Vanicky, I., 2021. A method to prepare large resin sections for counting myelinated axons in rodent CNS and PNS structures. Neurosci. Lett. 750, 135767.
Grinsell, D., Keating, C.P., 2014. Peripheral nerve reconstruction after injury: a review of clinical and experimental therapies. Biomed. Res Int 2014, 698256.
Irintchev, A., 2011. Potentials and limitations of peripheral nerve injury models in rodents with particular reference to the femoral nerve. Ann. Anat. 193, 276–285.
Kallio, P.K., 1993. The results of secondary repair of 254 digital nerves. J. Hand Surg. Br. 18, 327–330.
Kaplan, H.M., Mishra, P., Kohn, J., 2015. The overwhelming use of rat models in nerve regeneration research may compromise designs of nerve guidance conduits for humans. J. Mater. Sci. Mater. Med 26, 226.
Koller, R., Rab, M., Todoroff, B.P., Neumayer, C., Haslik, W., Stohr, H.G., Frey, M., 1997. The influence of the graft length on the functional and morphological result after nerve grafting: an experimental study in rabbits. Br. J. Plast. Surg. 50, 609–614.
Konofaos, P., Ver Halen, J.P., 2013. Nerve repair by means of tubulization: past, present, future. J. Reconstr. Microsurg 29, 149–164.
Kornfeld, T., Vogt, P.M., Radtke, C., 2019. Nerve grafting for peripheral nerve injuries with extended defect sizes. Wien. Med Woche 169, 240–251.
Leandri, M., Saturno, M., Cilli, M., Bisaglia, M., Lunardi, G., 2007. Compound action potential of sensory tail nerves in the rat. Exp. Neurol. 203, 148–157.
Leandri, M., Leandri, S., Lunardi, G., 2008. Effect of temperature on sensory and motor conduction of the rat tail nerves. Neurophysiol. Clin. 38, 297–304.
Loffredo, M.A., Yan, J.G., Kao, D., Zhang, L.L., Matloub, H.S., Riley, D.A., 2009. Persistent reduction of conduction velocity and myelinated axon damage in vibrated rat tail nerves. Muscle Nerve 39, 770–775.
Pan, D., Mackinnon, S.E., Wood, M.D., 2020. Advances in the repair of segmental nerve injuries and trends in reconstruction. Muscle Nerve 61, 726–739.
Panagopoulos, G.N., Megaloikonomos, P.D., Mavrogenis, A.F., 2017. The present and future for peripheral nerve regeneration. Orthopedics 40, e141–e156.
Poppler, L.H., Ee, X., Schellhardt, L., Hoben, G.M., Pan, D., Hunter, D.A., Yan, Y., Moore, A.M., Snyder-Warwick, A.K., Stewart, S.A., Mackinnon, S.E., Wood, M.D., 2016. Axonal growth arrests after an increased accumulation of schwann cells expressing senescence markers and stromal cells in acellular nerve allografts. Tissue Eng. Part A 22, 949–961.
Rbia, N., Shin, A.Y., 2017. The role of nerve graft substitutes in motor and mixed motor/sensory peripheral nerve injuries. J. Hand Surg. Am. 42, 367–377.
Riccio, M., Marchesini, A., Pugliese, P., De, F., 2019. Francesco, Nerve repair and regeneration: Biological tubulization limits and future perspectives. J. Cell Physiol. 234, 3362–3375.
Sahakyants, T., Lee, J.Y., Friedrich, P.F., Bishop, A.T., Shin, A.Y., 2013. Return of motor function after repair of a 3-cm gap in a rabbit peroneal nerve: a comparison of autograft, collagen conduit, and conduit filled with collagen-GAG matrix. J. Bone Jt. Surg. Am. 95, 1952–1958.
Saheb-Al-Zamani, M., Yan, Y., Farber, S.J., Hunter, D.A., Newton, P., Wood, M.D., Stewart, S.A., Johnson, P.J., Mackinnon, S.E., 2013. Limited regeneration in long acellular nerve allografts is associated with increased Schwann cell senescence. Exp. Neurol. 247, 165–177.
Scholz, T., Krichevsky, A., Sumarto, A., Jaffurs, D., Wirth, G.A., Paydar, K., Evans, G.R., 2009. Peripheral nerve injuries: an international survey of current treatments and future perspectives. J. Reconstr. Microsurg 25, 339–344.
Vanicky, I., Blasko, J., Koncekova, J., Dzurjaskova, Z., Michalova, Z., Szekiova, E., 2022. Formaldehyde-hardened albumin as a non-penetrating embedding matrix for frozen and vibratome sectioning. Acta Histochem 124, 151838.
Vasudevan, S., Yan, J.G., Zhang, L.L., Matloub, H.S., Cheng, J.J., 2013. A rat model for long-gap peripheral nerve reconstruction. Plast. Reconstr. Surg. 132, 871–876.
Wang, B.B., Guo, C., Sun, S.Q., Zhang, X.N., Li, Z., Li, W.J., Li, Z., Schumacher, M., Liu, S., 2023. Comparison of the nerve regeneration capacity and characteristics between sciatic nerve crush and transection injury models in rats. Biomed. Environ. Sci. 36, 160–173.
Weber, R.A., Proctor, W.H., Warner, M.R., Verheyden, C.N., 1993. Autotomy and the sciatic functional index. Microsurgery 14, 323–327.
Zygelyte, E., Bernard, M.E., Tomlinson, J.E., Martin, M.J., Terhorst, A., Bradford, H.E., Lundquist, S.A., Sledziona, M., Cheetham, J., 2016. RetroDISCO: Clearing technique to improve quantification of retrograde labeled motor neurons of intact mouse spinal cords. J. Neurosci. Methods 271, 34–42.